

# Possible $S_{\pm}$ -wave superconductivity in $\text{La}_3\text{Ni}_2\text{O}_7$

Qing-Geng Yang,<sup>1</sup> Han-Yang Liu,<sup>1</sup> Da Wang,<sup>1,2</sup> and Qiang-Hua Wang<sup>1,2,\*</sup>

<sup>1</sup>*National Laboratory of Solid State Microstructures & School of Physics, Nanjing University, Nanjing, 210093, China*

<sup>2</sup>*Collaborative Innovation Center of Advanced Microstructures, Nanjing 210093, China*

Recently, the bulk nickelate  $\text{La}_3\text{Ni}_2\text{O}_7$  is reported to show signature of high-temperature superconductivity under high pressure above 14GPa (H. Sun *et al.*, arXiv:2305.09586). We analyze the pairing mechanism and pairing symmetry in a bi-layer Hubbard model with two orbitals in the  $E_g$  multiplet. In the weak to moderate interaction regime, our functional renormalization group calculations yield  $S_{\pm}$ -wave Cooper pairing with dominant  $d_{3z^2-r^2}$ -orbital content, triggered by spin fluctuations at wave vectors near  $(0.84, 0)\pi$  and  $(0.75, 0.75)\pi$ , up to  $C_{4v}$  symmetry. The gap function changes sign across the Fermi pockets. In the strong coupling limit, we develop a low-energy effective theory in terms of atomic one- and two-electron states in the  $E_g$  multiplet. The effective theory predicts naturally local pairing (with anti-phase between the two orbitals due to the repulsive inter-orbital pair hopping) and strong singlet pairing on vertical inter-layer bond, where the super-exchange between  $d_{3z^2-r^2}$ -orbital is the strongest. The real-space structure is consistent with that from functional renormalization group, suggesting the robustness of such a pairing function. We also discuss a possible scenario for the weak insulating behavior under low pressures in terms of the tendency toward the formation of charge order in the strong coupling limit.

## I. INTRODUCTION

After the discovery of cuprate high- $T_c$  superconductors [1, 2], there are continuing efforts to search for superconductivity in perovskites of similar structure, such as ruthenates [3], cobaltates [4] and nickelates [5], in order to understand how unique the copper is in cuprates on one hand, and to discover new families of high- $T_c$  superconductors on the other hand. As a possible breakthrough along this line, a recent report shows signature of superconductivity in the bulk nickelate  $\text{La}_3\text{Ni}_2\text{O}_7$  with  $T_c$  as high as 80K at a pressure above 14GPa [6]. It has a bi-layer perovskite structure with the nickel atom sitting in the center of each oxygen octahedron, with layered  $\text{NiO}_2$ -plane similar to the  $\text{CuO}_2$ -plane in cuprates. However, the valence of Ni-atom fluctuates between  $\text{Ni}^{2+}$  and  $\text{Ni}^{3+}$ , with an average  $3d^{7.5}$  atomic configuration. Under high pressure, both  $3d_{x^2-y^2}$ - and  $3d_{3z^2-r^2}$ -orbitals in the  $E_g$ -multiplets are active near the Fermi level [6, 7]. The  $E_g$  multiplets in  $\text{La}_3\text{Ni}_2\text{O}_7$  is also different to the  $t_{2g}$  multiplets in iron-based superconductors [8, 9] where the Fe-atom is in an edge-sharing tetrahedra. At the fractional filling,  $\text{La}_3\text{Ni}_2\text{O}_7$  is unlikely to form a Mott insulator. But quite unexpectedly, the material is weakly insulating at lower pressures [6].

The novel attributes of  $\text{La}_3\text{Ni}_2\text{O}_7$  motivate us to explore the pairing mechanism and pairing symmetry therein, and to understand the weak insulating behavior under lower pressures. We perform the analysis within a bi-layer two-orbital Hubbard model

by functional renormalization group (FRG) in the weak to moderate interaction regime, and effective theory in the strong coupling limit. We find the Cooper pairing has  $S_{\pm}$ -wave symmetry. In momentum space, the sign change of the gap function is compatible with the structure of leading spin fluctuations, suggesting pairing triggered by spin fluctuations. In real space, the Cooper pair is composed of intra-orbital pairing on-site and on the vertical inter-layer bond, with stronger amplitudes in the  $d_{3z^2-r^2}$ -orbital content, anti-phase between the on-site and on-bond pairs, and anti-phase between the on-site pairs. In the strong coupling limit, we develop a low-energy effective theory in terms of atomic one- and two-electron states in the  $E_g$  multiplet. The real-space feature of the Cooper pair from FRG can be understood naturally in the strong coupling theory, with the strongest super-exchange between  $d_{3z^2-r^2}$ -orbitals on the vertical bonds, and the on-site repulsive inter-orbital pair hopping. We also discuss a possible scenario of the weak insulating behavior under lower pressures in terms of the tendency toward charge ordering in the strong coupling limit.

## II. MODEL

We start from a two-orbital ( $d_{3z^2-r^2}$  and  $d_{x^2-y^2}$ ) tight-binding model on a bi-layer square lattice as extracted from the Wannier fitting to the band structure of density functional theory (DFT) [7],

$$H_0 = \sum_{ia,jb,\sigma} t_{ij}^{ab} c_{ia\sigma}^\dagger c_{jb\sigma} + \sum_{ia\sigma} \varepsilon_a c_{ia\sigma}^\dagger c_{ia\sigma}, \quad (1)$$

where  $i, j$  are site indices,  $a, b$  are orbital indices,  $\sigma$  denotes spin,  $t_{ij}^{ab}$  is the hopping matrix element

\* qhwang@nju.edu.cn

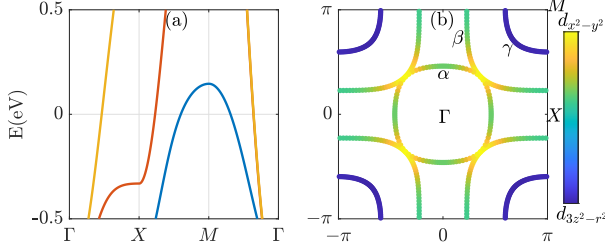


FIG. 1. (a) Band dispersion along the high symmetry lines  $\Gamma - X - M - \Gamma$ . (b) Fermi surfaces in the first Brillouin zone with the orbital characters indicated by colors. The three pockets are labeled by  $\alpha$ ,  $\beta$  and  $\gamma$ , respectively.

between  $ia$  and  $jb$ ,  $\varepsilon_a$  is the on-site energy of the  $a$ -orbital. The parameters are taken from Ref. [7]. We note that the hopping of  $d_{3z^2-r^2}$ -electron along the vertical inter-layer bond is the strongest.

The energy bands (a) and Fermi surfaces (b) are shown in Fig. 1. There are three bands crossing the Fermi level, leading to three Fermi pockets: one electron  $\alpha$ -pocket around  $\Gamma$ , one hole  $\gamma$ -pocket around  $M$ , and another large  $\beta$ -pocket also surrounding  $M$  which nearly touches the  $\alpha$ -pocket in the  $\Gamma - M$  directions (because of the minute inter-layer hopping of the  $d_{x^2-y^2}$ -orbital). From the color scale in Fig. 1(b), both the  $\alpha$ - and  $\beta$ -pockets show strong orbital hybridizations, while the  $\gamma$ -pocket mainly comes from the  $d_{3z^2-r^2}$ -orbital. From the DFT calculations, the shallow  $\gamma$ -pocket only appears in the high pressure phase, while it vanishes in the low pressure phase [6], suggesting its importance for superconductivity in this material.

We consider the multi-orbital atomic Coulomb interactions

$$H_I = \sum_{ia} U n_{ia\uparrow} n_{ia\downarrow} + \sum_{i,a\neq b} J_P c_{ia\uparrow}^\dagger c_{ia\downarrow}^\dagger c_{ib\downarrow} c_{ib\uparrow} + \frac{1}{2} \sum_{i,a\neq b,\sigma\sigma'} \left( U' n_{ia\sigma} n_{ib\sigma'} + J_H c_{ia\sigma}^\dagger c_{ib\sigma} c_{ib\sigma'}^\dagger c_{ia\sigma'} \right), \quad (2)$$

where  $U$  is the intra-orbital Hubbard repulsion,  $U'$  is the inter-orbital Coulomb interaction,  $J_H$  is the Hund's coupling, and  $J_P$  is the pair hopping interaction. Throughout this work, we use the Kanamori relations [10]  $U = U' + 2J_H$  and  $J_H = J_P$ .

### III. FUNCTIONAL RENORMALIZATION GROUP

We first perform the singular-mode functional renormalization group (SM-FRG) [11, 12] calculations to look for possible electronic instabilities in

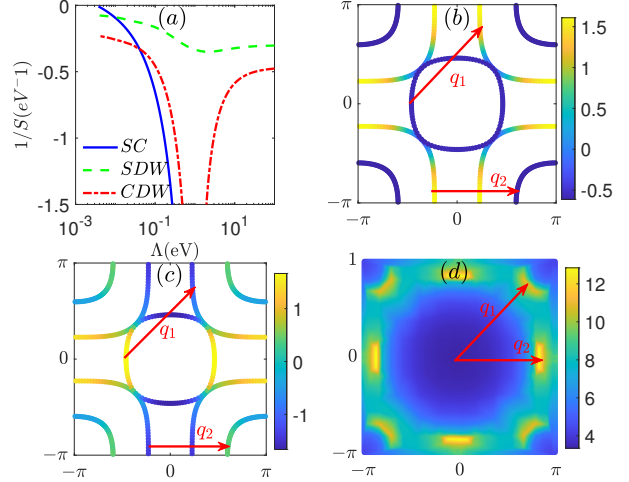


FIG. 2. (a) FRG flows of  $1/S$  with respect to the RG energy scale  $\Lambda$  for the SC, SDW and CDW channels, respectively. (b) and (c) plot the leading  $s$ -wave and subleading  $d_{x^2-y^2}$ -wave pairing functions projected to the Fermi surfaces encoded by colors. (d) plot the renormalized  $V_{\text{SDW}}(\mathbf{q})$ . The two peaks are labeled as  $\mathbf{q}_{1,2}$ , corresponding to the transferring momentum connecting opposite pairing signs as indicated in (b) and (c).

the system. The FRG approach is controlled in the weak to moderate interaction regime. It provides the flow of the effective interactions between quasi-particles versus a running infrared cutoff energy scale  $\Lambda$  (the lowest Matsubara frequency in our case). As  $\Lambda$  is lowered from the ultra-violet limit, we extract from the full effective interactions the scattering matrices  $V_{\text{SC,SDW,CDW}}(\mathbf{q})$  between fermion bilinears (of momentum  $\mathbf{q}$ ) in the superconducting (SC), spin-density-wave (SDW) and charge-density-wave (CDW) channels, respectively. As an example, in real space,  $c_{a\sigma}^\dagger(\mathbf{R})c_{b\sigma'}^\dagger(\mathbf{R} + \mathbf{b})$  is a bilinear for the creation of a fermion pair in the SC channel, labelled by the orbital-spin combination  $(a\sigma, b\sigma')$  and the internal displacement  $\mathbf{b}$ , in addition to the shared position  $\mathbf{R}$ . Similar bilinears can be defined in other channels, and are transformed into the momentum space in the calculations. We trace the leading negative eigenvalue  $S$  in each channel. The first divergence at a critical scale  $\Lambda = \Lambda_c$  signals an emerging electronic order at transition temperature  $T_c \sim \Lambda_c$ , described by the bilinear combination in the eigen scattering mode of the diverging channel. The details of our SM-FRG can be found in Refs. [11, 13–15].

A typical FRG flow is shown in Fig. 2(a), where we plot  $1/S$  versus  $\Lambda$  for the case of  $(U, J_H) = (3, 0.3)\text{eV}$ . The SDW channel is strongest at high energy scales, as in the bare interaction. The CDW channel is initially reduced by Coulomb screening,

which also causes the SDW channel to decrease slightly. The SC channel does not show up initially since it is repulsive. The SDW channel begins to increase further as  $\Lambda \sim 1\text{eV}$ , as off-site spin correlations are induced. Meanwhile, through the channel overlap, the SDW channel triggers the rise of the SC channel. This is a manifestation of the well-known Kohn-Luttinger mechanism [16]. The CDW also rises because off-site bilinears (such as the valence bond) in this channel can be induced by SDW. Note that cusps or dips in the flow are a signature of level crossing between the leading (shown) and subleading (not shown) scattering modes. As  $\Lambda$  is lowered further, the SDW and CDW channels tend to saturate because the phase space for low-energy particle-hole excitations decreases. However, the SC channel at zero bilinear momentum  $\mathbf{q} = 0$  can continue to rise through the Cooper mechanism. Finally the SC channel diverges first, suggesting an instability of the normal state toward the SC state.

We next analyze the resulting pairing order parameter. The Cooper pair from the leading bilinear eigen mode of  $V_{\text{SC}}$  turns out to be dominated by, in real space, intra-orbital spin singlet within the unit cell, as illustrated in the inset of Fig. 3, with the following components for the case of  $(U, J_H) = (3, 0.3)\text{eV}$ : (i) the pairing between  $d_{3z^2-r^2}$ -orbitals with onsite amplitude  $u_0 = -0.43$  and vertical-bond amplitude  $u_1 = 0.51$ , and (ii) the pairing between the  $d_{x^2-y^2}$ -orbitals with onsite amplitude  $v_0 = 0.14$  and vertical-bond amplitude  $v_1 = 0.07$ . The pairing between the  $d_{3z^2-r^2}$ -orbitals are much stronger. The anti-phase between the two onsite pairing amplitudes is consistent with the repulsive bare local pair hopping interaction. The pairing symmetry is clearly  $S$ -wave. To gain more insights, we project the pairing function into the band basis, and show the gap function on the Fermi surfaces in Fig. 2(b). Both  $\alpha$ - and  $\gamma$ -pockets are fully gapped with the same sign, while the gap on the  $\beta$ -pocket is largely of opposite sign and diminishes in the nodal direction where the two pockets are very close. Therefore, exactly speaking, the pairing symmetry is  $S_{\pm}$ -wave, similarly to the case in iron pnictides [17]. We should note that as the leading eigen mode diverges, the second-leading one is finite, and can be ruled out as a competitor for the SC state. However, for comparison, we also plot the gap function for the second-subleading eigen mode in Fig. 2(c), which clearly has the  $d_{x^2-y^2}$ -wave symmetry. However, since the  $\gamma$ -pocket is near  $M$ , the  $d_{x^2-y^2}$ -wave gap function is tiny on the entire  $\gamma$  pocket. This should be unfavorable to gain condensation energy if such a pairing would occur in the SC state. Interestingly, the experiment shows that the SC phase appears when the  $\gamma$ -pocket appears [6]. This fact supports our  $S_{\pm}$ -

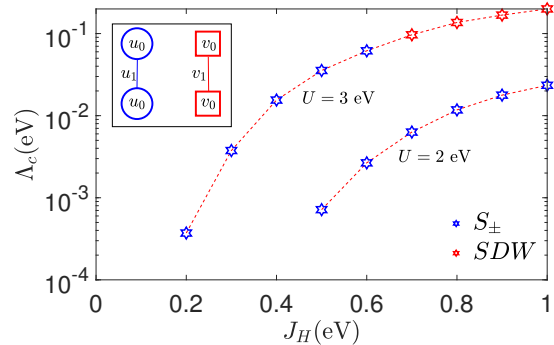


FIG. 3. The critical scales  $\Lambda_c$  are plotted versus  $J_H$  for two fixed values of  $U$ . Blue and green stars stand for  $S_{\pm}$ -wave SC and SDW, respectively. The inset illustrates the pairing structure with mainly intra-orbital components:  $u_{0,1}$  between  $d_{3z^2-r^2}$ -orbitals and  $v_{0,1}$  between  $d_{x^2-y^2}$ -orbitals.

wave instead of  $d_{x^2-y^2}$ -wave pairing as the leading pairing symmetry.

In Fig. 2(d), we plot the leading negative eigenvalue of the renormalized  $V_{\text{SDW}}(\mathbf{q})$  in the momentum space. We see the spin interaction is strong near momenta  $\mathbf{q}_1 \sim (0.75, 0.75)\pi$  and  $\mathbf{q}_2 \sim (0.84, 0)\pi$ , up to symmetry related images, which appear to connect the Fermi points where the gap function has opposite sign, see the arrows in Fig. 2(b) and (c). This is consistent with pairing triggered by spin fluctuations, as the FRG flow already suggests. Similar mechanism is believed to work in cuprates and iron pnictides, at least in the weak-coupling scenario [18].

To see how robust is the  $S_{\pm}$ -wave pairing, we performed systematic calculations by varying  $J_H$  and  $U$ , with  $J_H \leq U/2$ . Fig. 3 shows the phase diagram. We find the  $S_{\pm}$ -wave pairing is always favored, and the critical scale increases with  $J_H$ , until the SDW channel begins to win for larger  $U$  and  $J_H$ . The reason is the SDW interaction is enhanced by  $J_H$ , even at the bare level. While the exact values for  $U$  and  $J_H$  are unavailable at this stage, our results show that the SC phase is realized in a large regime of the parameter space.

#### IV. STRONG COUPLING LIMIT

While the FRG works in the weak to moderate interaction regime, it is likely that the actual interaction is large and falls in the strong coupling limit. It is therefore interesting to ask what would happen in this limit. We begin by specifying the appropriate low energy manifold for the specific filling level  $3/2$ . For simplicity, we first assume  $U = U'$  and set  $J_H = J_P = 0$ . (The difference to this situation will be taken as perturbations.) In the atomic limit,

the 1e- and 2e-states, with one and two electrons on the two orbitals, become degenerate and have energy  $-U$ , if the chemical potential is set at  $\mu = U$ , while the energy of the 0e- and 3e-states is 0, and the 4e-state has even higher energy  $2U$  and can be ignored. These atomic levels are sketched in Fig. 4(a). So the ground state manifold is spanned by the 1e- and 2e-states, and the density of both atomic states should be 1/2 to match the average electron filling level 3/2. Now switch on the kinetic hoppings and project to the Hilbert space in the ground state manifold, the effective Hamiltonian can be written as

$$\tilde{H} = PH_0P + PH_1P - \frac{1}{U}PH_tQH_tP, \quad (3)$$

where  $P$  is the projection operator for the 1e- and 2e-states,  $H_t$  is the kinetic hopping part of  $H_0$ , and  $Q$  is the projection operator for an intermediate single 0e- or 3e-state. We take  $\bar{U} = (U + U')/2$  to approximate the energy of such a state. The projected Hamiltonian contains the following terms: (i) The hopping  $Pc_{ia\sigma}^\dagger c_{jb\sigma}P$  can occur only if site  $j$  is previously in the 2e-state, and site  $i$  in the 1e-state. See Fig. 4(b). After the hopping the two charge states exchanges. This restriction should lead to significant reduction in the band width. (ii) The local interaction is only allowed for the 2e-states. The local pair hopping between the two orbitals is unaffected by projection. Since it is repulsive, it requires the local intra-orbital pairing on the two orbitals to develop anti-phase in the SC state. (iii) The super-exchange is limited to that between two 2e-states, or between two 1e-states, see Fig. 4(c) and (d). The super-exchange between 1e- and 2e-states would lead to an intermediate state with both 0e- and 3e-states, which is too high in energy. On the other hand, since the inter-orbital hopping is small, and since the product of two intra-orbital hoppings involving two different orbitals is also small, the leading super-exchange is through two intra-orbital hoppings involving the same orbital. Among other effects, the super-exchange can lead to anti-ferromagnetic spin-spin interaction, and the strongest one is on the vertical bond for the  $d_{3z^2-r^2}$ -orbital where the hopping amplitude is the largest. This interaction can lead to singlet pairing on the vertical bond. The pairing tendencies in (ii) and (iii) are consistent with the FRG result in the previous section. A renormalized mean field theory in the Gutzwiller approximation [19–21] for the projected Hamiltonian will be presented elsewhere.

Finally, we recall that in a usual one-band Hubbard model on the square lattice, the nearest-neighbor Coulomb interaction  $V$  would favor a charge ordered state provided that  $V > U/4$  [22]. However, in the above projected Hamiltonian suitable for the average 3/2-filling, the 1e- and 2e-states

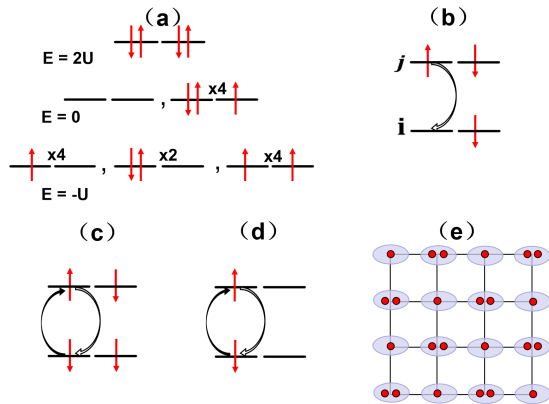


FIG. 4. (a) Atomic energy levels for 3/2-filling. The degeneracy for each configuration is labeled out. (b) shows the hopping process  $Pc_{ia\sigma}^\dagger c_{ja\sigma}P$ . (c) and (d) illustrate the super-exchange processes between two 2e-states and between two 1e-states, respectively. (e) is a scheme of the charge order in one plane.

are near degenerate at the atomic level, so that  $U$  does not hamper the charge ordering of the 1e- and 2e-states. On the other hand, the  $V$ -interaction can be written as  $V \sum_{\langle ij \rangle} (n_i - 1)(n_j - 1)$ , where we subtracted a reference unit charge without changing the physics at the fixed average filling. From this we see that it is advantageous to form a staggered charge order of 1e- and 2e-states on the lattice, a form of Wigner crystal, see Fig. 4(e), to gain Coulomb energy. The charge order only has to fight against the kinetic quantum fluctuations, and would set in once  $4V\chi_c \geq 1$  in the simple Peierls picture, where  $\chi_c$  is the charge susceptibility. In the present case, the projection reduces the bandwidth and enhances the charge susceptibility. More interestingly, at lower pressures the bare bandwidth should be smaller, so that the charge order is more likely to occur. The charge order reduces the charge mobility and the transition may be first order. This may explain the weak insulating behavior at lower pressures, and the abrupt emergence of the SC state at higher pressures [6].

## V. SUMMARY AND DISCUSSION

To conclude, we discussed the pairing mechanism and pairing symmetry in  $\text{La}_3\text{Ni}_2\text{O}_7$  by FRG in the weak to moderate interaction regime, and effective theory in the strong coupling limit. We find the Cooper pairing has  $S_{\pm}$ -wave symmetry, with gap sign change on the Fermi surfaces consistent with strong spin fluctuations. In real space, the Cooper

pair is composed of intra-orbital pairing within the unit cell, dominated by the  $d_{3z^2-r^2}$ -orbital content, and has anti-phase between the on-site and on-bond pairs, and anti-phase between the on-site pairs. This form of local pairing is argued to be robust also in the strong coupling limit, for which we develop a low-energy effective theory in terms of atomic 1e- and 2e-states in the  $E_g$  multiplet. We also discuss

a possible scenario of the weak insulating behavior under lower pressures in terms of the tendency toward charge ordering of the atomic 1e- and 2e-states in the strong coupling limit.

This work is supported by National Key R&D Program of China (Grant No. 2022YFA1403201) and National Natural Science Foundation of China (Grant No. 12274205 and No. 11874205).

- 
- [1] J. G. Bednorz and K. A. Müller, Possible high Tc superconductivity in the Ba-La-Cu-O system, *Z. Physik B - Condensed Matter* **64**, 189 (1986).
- [2] P. A. Lee, N. Nagaosa, and X.-G. Wen, Doping a Mott insulator: Physics of high-temperature superconductivity, *Rev. Mod. Phys.* **78**, 17 (2006).
- [3] Y. Maeno, H. Hashimoto, K. Yoshida, S. Nishizaki, T. Fujita, J. G. Bednorz, and F. Lichtenberg, Superconductivity in a layered perovskite without copper, *Nature* **372**, 532 (1994).
- [4] K. Takada, H. Sakurai, E. Takayama-Muromachi, F. Izumi, R. A. Dilanian, and T. Sasaki, Superconductivity in two-dimensional CoO<sub>2</sub> layers, *Nature* **422**, 53 (2003).
- [5] D. Li, K. Lee, B. Y. Wang, M. Osada, S. Crossley, H. R. Lee, Y. Cui, Y. Hikita, and H. Y. Hwang, Superconductivity in an infinite-layer nickelate, *Nature* **572**, 624 (2019).
- [6] H. Sun, M. Huo, X. Hu, J. Li, Y. Han, L. Tang, Z. Mao, P. Yang, B. Wang, J. Cheng, D.-X. Yao, G.-M. Zhang, and M. Wang, Superconductivity near 80 Kelvin in single crystals of La<sub>3</sub>Ni<sub>2</sub>O<sub>7</sub> under pressure (2023), [arXiv:2305.09586 \[cond-mat.supr-con\]](https://arxiv.org/abs/2305.09586).
- [7] Z. Luo, X. Hu, M. Wang, W. Wú, and D.-X. Yao, Bilayer two-orbital model of La<sub>3</sub>Ni<sub>3</sub>O<sub>7</sub> under pressure (2023), [arXiv:2305.15564 \[cond-mat.supr-con\]](https://arxiv.org/abs/2305.15564).
- [8] Y. Kamihara, T. Watanabe, M. Hirano, and H. Hosono, Iron-Based Layered Superconductor La[O<sub>1-x</sub>F<sub>x</sub>]FeAs ( $x=0.05-0.12$ ) with T<sub>c</sub>=26K, *J. Am. Chem. Soc.* **130**, 3296 (2008).
- [9] G. R. Stewart, Superconductivity in iron compounds, *Rev. Mod. Phys.* **83**, 1589 (2011).
- [10] C. Castellani, C. R. Natoli, and J. Ranninger, Magnetic structure of v<sub>2</sub>o<sub>3</sub> in the insulating phase, *Phys. Rev. B* **18**, 4945 (1978).
- [11] W.-S. Wang, Y.-Y. Xiang, Q.-H. Wang, F. Wang, F. Yang, and D.-H. Lee, Functional renormalization group and variational Monte Carlo studies of the electronic instabilities in graphene near 1/4 doping, *Phys. Rev. B* **85**, 035414 (2012).
- [12] Y.-Y. Xiang, F. Wang, D. Wang, Q.-H. Wang, and D.-H. Lee, High-temperature superconductivity at the FeSe/SrTiO<sub>3</sub> interface, *Phys. Rev. B* **86**, 134508 (2012).
- [13] W. Metzner, M. Salmhofer, C. Honerkamp, V. Meden, and K. Schönhammer, Functional renormalization group approach to correlated fermion systems, *Rev. Mod. Phys.* **84**, 299 (2012).
- [14] W.-S. Wang, Z.-Z. Li, Y.-Y. Xiang, and Q.-H. Wang, Competing electronic orders on kagome lattices at van Hove filling, *Phys. Rev. B* **87**, 115135 (2013).
- [15] Q.-K. Tang, L. Yang, D. Wang, F.-C. Zhang, and Q.-H. Wang, Spin-triplet  $f$ -wave pairing in twisted bilayer graphene near 1/4-filling, *Phys. Rev. B* **99**, 094521 (2019).
- [16] W. Kohn and J. M. Luttinger, New Mechanism for Superconductivity, *Phys. Rev. Lett.* **15**, 524 (1965).
- [17] A. Chubukov, Pairing Mechanism in Fe-Based Superconductors, *Annu. Rev. Condens. Matter Phys.* **3**, 57 (2012).
- [18] D. J. Scalapino, A common thread: The pairing interaction for unconventional superconductors, *Rev. Mod. Phys.* **84**, 1383 (2012).
- [19] M. C. Gutzwiller, Effect of Correlation on the Ferromagnetism of Transition Metals, *Phys. Rev. Lett.* **10**, 159 (1963).
- [20] Q.-H. Wang, Z. Wang, Y. Chen, and F. Zhang, Unrestricted renormalized mean field theory of strongly correlated electron systems, *Phys. Rev. B* **73**, 092507 (2006).
- [21] B. Edeger, V. N. Muthukumar, and C. Gros, Gutzwiller–RVB theory of high-temperature superconductivity: Results from renormalized mean-field theory and variational Monte Carlo calculations, *Adv. Phys.* **56**, 927 (2007).
- [22] M. Yao, D. Wang, and Q.-H. Wang, Determinant quantum monte carlo for the half-filled hubbard model with nonlocal density-density interactions, *Phys. Rev. B* **106**, 195121 (2022).